5332574

ACCEPTED FOR PUBLICATION IN THE ASTROPHYSICAL JOURNAL LETTERS
Preprint typeset using LaTeX style emulateapj v. 14/09/00

arXiv:astro-ph/0010356 18 Oct 2000

HIGH-RESOLUTION X-RAY SPECTROSCOPY OF THE SEYFERT 2 GALAXY CIRCINUS WITH *Chandra*

RITA M. SAMBRUNA,[1] HAGAI NETZER,[2] SHAI KASPI,[1] W. N. BRANDT,[1] G.CHARTAS,[1] G.P.GARMIRE,[1]
JOHN A. NOUSEK,[1] AND K.A.WEAVER,[3]
Accepted for publication in the Astrophysical Journal Letters

ABSTRACT

Results from a 60 ks *Chandra* HETGS observation of the nearby Seyfert 2 Circinus are presented. The spectrum shows a wealth of emission lines at both soft and hard X-rays, including lines of Ne, Mg, Si, S, Ar, Ca, and Fe, and a prominent Fe Kα line at 6.4 keV. We identify several of the He-like components and measure several of the Lyman lines of the H-like ions. The lines' profiles are unresolved at the limited signal-to-noise ratio of the data. Our analysis of the zeroth-order image in a companion paper constrains the size of the emission region to be 20–60 pc, suggesting that emission within this volume is almost entirely due to the reprocessing of the obscured central source. Here we show that a model containing two distinct components can reproduce almost all the observed properties of this gas. The ionized component can explain the observed intensities of the ionized species, assuming twice-solar composition and an $N \propto r^{-1.5}$ density distribution. The neutral component is highly concentrated, well within the 0.8″ point source, and is responsible for almost all of the observed Kα (6.4 keV) emission. Circinus seems to be different than Mkn 3 in terms of its gas distribution.

Subject headings: galaxies: active — galaxies: nuclei — galaxies: Seyfert — galaxies: individual (Circinus) — X-rays: galaxies

1. INTRODUCTION

Recent X-ray studies of Seyfert 2 galaxies with *ASCA* and *BeppoSAX* have shown that the 0.1–10 keV spectra of these sources are rich in emission lines at both soft and hard energies (e.g., Guainazzi et al. 1999; Turner et al. 1997). The interpretation of the emission lines is problematic because of ambiguities about line blending, line profiles, and line flux distribution that are all poorly constrained by *ASCA* and *BeppoSAX*. The data are consistent with emission from gas in photoionization equilibrium (e.g., Netzer, Turner, & George 1998 and references therein), but there are also attempts to fit the spectra by a two-temperature gas in collisional equilibrium (Ueno et al. 1994), presumably due to starburst emission. X-ray observations at high resolution both spatially and spectrally are crucial to determining the origin of the X-ray lines in Seyfert 2s, a task for which *Chandra* is uniquely suited.

Here we present a 60 ks *Chandra* HETGS spectrum of the Seyfert 2 galaxy Circinus. Previous *ASCA* and *BeppoSAX* observations of this source revealed several emission lines at both soft and hard energies (Sako et al. 2000a; Guainazzi et al. 1999; Matt et al. 1996). In a companion paper, focusing on the zeroth-order ACIS image, we established that several components contribute to the X-ray emission from Circinus. In particular, we found that $\sim$ 60% of the X-ray flux at $\lesssim$ 2 keV is due to an extended component on scales $\sim$ 2.3″, while at harder energies the contribution from a compact ($\lesssim$ 0.8″) region prevails. Importantly, the ACIS spectrum of the latter component exhibits several emission lines including a prominent (EW $\sim$ 2.5 keV) Fe Kα line. In this paper, we concentrate on the analysis of the HETGS spectrum and on the implications for the physical conditions of the emitting gas. We also use a simultaneous *RXTE* observation to derive useful constraints on the intrinsic nuclear X-ray continuum. At the distance of the galaxy ($\sim$ 4 Mpc), 1″≃19 pc.

2. OBSERVATIONS AND DATA ANALYSIS

Circinus was observed with the High Energy Transmission Grating Spectrometer (HETGS; Canizares et al. 2000, in prep.) on 2000 June 6, with ACIS-S (Garmire et al. 2000) in the focal plane. The total net exposure was 60,223 s. Details on the observation are given in our companion paper.

The HETGS carries two mirror assemblies, the High Energy Grating (HEG) and Medium Energy Grating (MEG). The nuclear HEG and MEG spectra were extracted in a narrow (15 pixel) rectangular region centered on the zeroth-order position, avoiding contamination from the dispersed spectra of the nearby serendipitous sources. Although a few of the serendipitous sources exhibit emission lines in their ACIS spectra at both soft and hard X-rays, the 0.5–8 keV flux of the brightest one is a factor 5 weaker than the nucleus. We thus believe that contamination to the HETGS nuclear spectrum (in the regions of overlap of the dispersed spectra) is negligible. The HEG and MEG spectra were gain corrected and flux calibrated using Ancillary Response Files generated with the CIAO software. Only the first order HEG and MEG spectra were used for the analysis, as higher orders contain only a few ($\lesssim$ 3 per bin) counts and are not useful. The spectra were also corrected for cosmological redshift and Galactic absorption, $N_H^{Gal} = 3.3 \times 10^{21}$ cm^{-2} (Freeman et al. 1977).

3. SIMULTANEOUS *RXTE* OBSERVATIONS

We used a simultaneous 30 ks exposure with *RXTE* to constrain the higher-energy X-ray continuum emission from Circinus. The *RXTE* data were reduced following standard criteria; here we use only data from the PCA detector and report only on the results most relevant for the modeling of the *Chandra* HETGS data, leaving more details to a future paper. The source

[1] Department of Astronomy and Astrophysics, 525 Davey Laboratory, The Pennsylvania State University, University Park, PA 16802.
[2] School of Physics and Astronomy, Raymond and Beverly Sackler Faculty of Exact Sciences, Tel-Aviv University, Tel-Aviv 69978, Israel.
[3] Laboratory for High Energy Astrophysics, Code 660, NASA/Goddard Space Flight Center, Greenbelt, MD 20771.

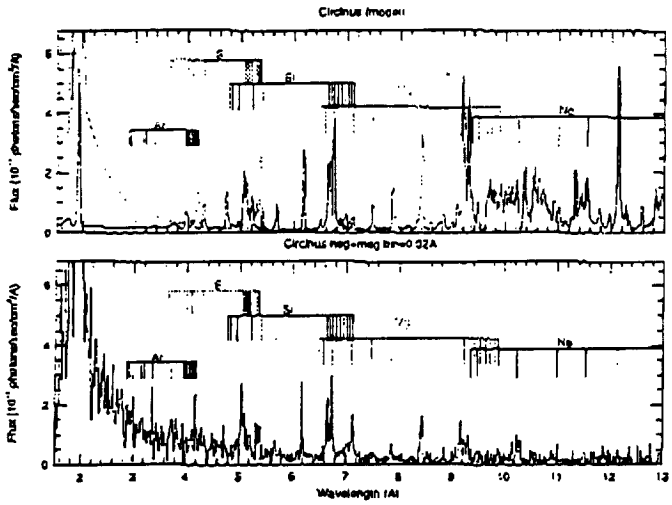

FIG. 1.— Bottom: The X-ray spectrum of Circinus from a 60 ks *Chandra* HETGS observation. The spectrum was obtained by averaging the MEG and HEG first-order spectra (after rebinning the HEG data to the same resolution as the MEG data), and rebinning to 0.02 Å. Many emission lines mostly due to H- and He-like elements are detected, together with weaker lines from "neutral" S, Si, and Ar. The most prominent feature is the Fe Kα line at 6.4 keV. Top: A two component model fit to the data: ionized component (solid line) and neutral component (dashed line).

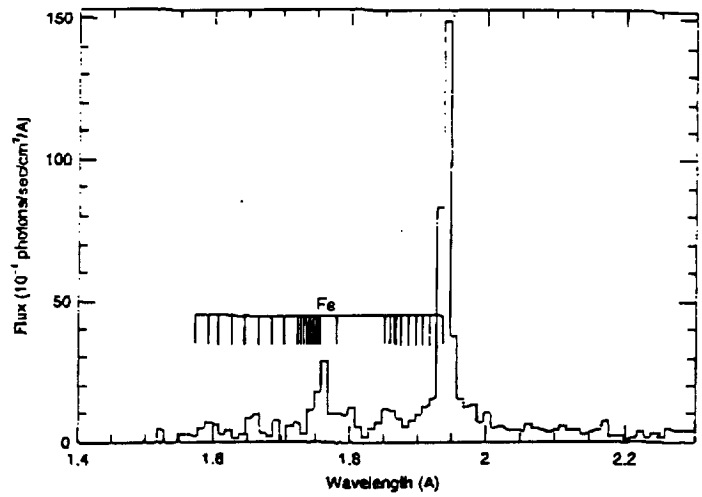

FIG. 2.— The Fe line complex in Circinus from a 60 ks HETGS exposure shown, this time, after rebinning to 0.01 Å. The Fe Kα line consists of a narrow, unresolved core plus a broader base. Also detected is the FeKβ line at 7.1 keV, and a weak line at 6.6 keV, with an energy consistent with Fe XXV.

was detected with the PCA up to ~ 30 keV, with a 2–30 keV count rate of 7.26 ± 0.04 counts s^{-1}.

We fitted the PCA data in the energy range 6–30 keV, where relatively few lines are present (mainly Fe Kα at 6.4 keV, FeKβ at 7.1 keV, and Fe XXVI/NiKα at 7.9 keV; Guainazzi et al. 1999). We find that an excellent description of the PCA data (χ^2=56 for 62 degrees of freedom) is obtained with a model including a "pure" reflection continuum from neutral gas, plus a heavily absorbed ($N_H \sim 6 \times 10^{24}$ cm^{-2}) power law dominant at $\gtrsim$ 10 keV, plus the three Gaussians lines. The best-fit model and fitted parameters are in complete agreement with a previous *BeppoSAX* observation of Circinus (Matt et al. 1999, Guainazzi et al. 1999). We mainly stress here the results for the intrinsic nuclear continuum: power-law photon index $\Gamma = 1.65^{+1.25}_{-0.35}$ (90% confidence errors) and intrinsic (absorption-corrected) 2–10 keV luminosity in the range $L^{intr}_{2-10\,keV} = 3 \times 10^{40} - 3 \times 10^{42}$ erg s^{-1}, in agreement with the *BeppoSAX* data (Matt et al. 1999).

4. THE HETGS SPECTRUM

The first order MEG spectra agree well with each other within the resolution of the grating (~ 0.023 Å, twice as for the HEG). The two HEG spectra also agree with each other and with the MEG spectra. Therefore, in order to increase the signal-to-noise ratio, the four spectra were averaged after rebinning the HEG data to the MEG resolution. While this procedure sacrifices the higher resolution of the HEG, in most cases the lines are unresolved and the loss of resolution is thus well compensated by a cleaner detection of the lines.

Figure 1 shows a wide wavelength coverage view of the flux-calibrated spectrum, binned at 0.02 Å. A plethora of emission lines are apparent in the spectrum at all energies. The most prominent one is the Fe Kα line at 6.4 keV, with an EW ~ 2.1 keV, an unresolved core, and a hint of a broader-base component which will be discussed elsewhere. A detailed view of the Fe line complex (Figure 2) shows also the Fe Kβ line at ~ 7.1 keV, with an intensity of ~ 0.2 that of the Fe Kα line. We have identified another feature at around 6.6 keV, consistent with the Fe XXV Kα line. As shown below, our model cannot explain the intensity of this feature. The high absorption column in the direction to Circinus, and the relatively faint X-ray flux of the source, do not allow any clear line detections below ~ 1 keV.

Table 1 gives quantitative information about the detected emission lines, including the line identification (note some question marks due to uncertain identifications), measured fluxes, and EWs. Many H-like and He-like lines of Mg, Si, S and possibly Ar are detected in the spectrum, together with weaker "neutral" lines of Si, S, Ar, and perhaps Ca. The high resolution allows deblending of the forbidden, intercombination, and resonance lines of several of the He-like ions (Figure 1). The significance of the lines' detections can be judged from the corresponding uncertainties on the line fluxes. The poor signal-to-noise ratio did not allow a meaningful line-width determination, and all FWHMs are consistent with the instrumental resolution.

The EWs are calculated with respect to the total observed continuum, which was evaluated using two independent methods. First, we selected line-free regions of the spectrum (mostly above 2–3 keV), rebinned the data heavily, and fitted them with a smooth curve. Second, we used the zeroth-order spectrum from an extraction radius consistent with the extraction width of the HETGS spectrum (~ 3″). The latter was fitted with a power law plus free N_H, plus narrow (width=0.05 keV) Gaussians representing all the emission lines detected in the HETGS spectrum. Both methods gave consistent results. The 3-7 keV continuum can be described by an inverted power law with photon index $\Gamma \sim -0.8$ and flux $F_{2-10\,keV} \sim 7 \times 10^{-12}$ erg cm^{-2} s^{-1}. This continuum was used in the EW measurements. The uncertainty on the continuum flux is 22% or better at all wavelengths.

5. DISCUSSION

We modeled the observed spectrum using our new line measurements, as well as the information obtained from the radial flux distribution (from our companion paper) and the high en-

TABLE 1
X-RAY EMISSION LINES

Line and energy(eV) (1)	Wavelength (Å) (2)	Energy (keV) (3)	Flux ($\times 10^{-4}$ ph cm^{-2} s^{-1}) (4)	EW (eV) (5)	EW (Å) (6)
Ne X (1211)	10.236	1.211 ± 0.003	0.025 ± 0.015	24 ± 17	0.20 ± 0.14
Mg XI (1352)	9.171	1.352 ± 0.003	0.058 ± 0.017	63 ± 24	0.43 ± 0.16
Mg XI (1343)	9.245	1.341 ± 0.003	0.026 ± 0.013	28 ± 17	0.20 ± 0.12
Mg XI (1333)	9.300	1.332 ± 0.003	0.034 ± 0.016	36 ± 19	0.25 ± 0.13
Mg XII (1472)	8.419	1.471 ± 0.004	0.065 ± 0.016	77 ± 23	0.44 ± 0.13
Mg XI (1579)	7.851	1.578 ± 0.004	0.019 ± 0.013	23 ± 13	0.12 ± 0.08
Mg XII (1745)	7.106-7.130	1.741 ± 0.005	0.086 ± 0.017	116 ± 32	0.47 ± 0.13
+ Si II– VI(1740–1746)					
Si XIII (1865)	6.648	1.863 ± 0.006	0.087 ± 0.016	120 ± 23	0.43 ± 0.08
Si XIII (1839)	6.74 + 6.737	1.841 ± 0.006	0.105 ± 0.018	146 ± 38	0.54 ± 0.14
+ Mg XII (1840)					
Si XIV (2007)	6.180	2.006 ± 0.007	0.064 ± 0.015	91 ± 28	0.28 ± 0.09
S II– X(2308–2350)	5.28–5.37	2.313 ± 0.009	0.029 ± 0.032	43 ± 47	0.10 ± 0.11
Si XIV (2377)	5.217 + 5.194	2.383 ± 0.009	0.048 ± 0.037	71 ± 46	0.16 ± 0.10
+ S XII (2387)					
S XIV (2411)	5.142	2.412 ± 0.009	0.028 ± 0.027	42 ± 40	0.09 ± 0.08
S XV (2430)	5.100	2.433 ± 0.010	0.056 ± 0.029	83 ± 39	0.18 ± 0.09
S XV (2461)	5.039	2.458 ± 0.010	0.085 ± 0.036	125 ± 61	0.26 ± 0.13
S XVI (2623)	4.727	2.624 ± 0.011	0.022 ± 0.023	33 ± 35	0.06 ± 0.06
S XV (2883)	4.299	2.882 ± 0.011	0.021 ± 0.023	31 ± 34	0.05 ± 0.05
Ar II– XI (2962–2990)	4.12–4.187	2.960± 0.014	0.06 ± 0.031	83 ± 40	0.12 ± 0.06
Ar XVII (3104–3140)	3.949–3.994	3.683 ± 0.022	0.039 ± 0.021	54.2 ± 28.7	0.05 ± 0.03
Ar XVIII (3323)	3.794	3.268 ± 0.020	0.040 ± 0.024	59 ± 38	0.07 ± 0.05
Ar XVIII (3936)	3.150	3.917 ± 0.025	0.041 ± 0.026	55 ± 31	0.05 ± 0.03
Ca II– XIV(3690–3760)	3.30–3.36	3.683 ± 0.022	0.038 ± 0.021	53 ± 31	0.05 ± 0.03
+ Ar XVII (3684)					
Ca XX ? (5115)	2.424	5.166 ± 0.042	0.102 ± 0.040	127 ± 56	0.06 ± 0.03
?	2.606	4.758 ± 0.037	0.052 ± 0.029	64 ± 38	0.04 ± 0.02
?	2.069	5.993 ± 0.058	0.145 ± 0.054	177 ± 69	0.06 ± 0.02
Fe II– XVII(6400)	1.942	6.385 ± 0.066	3.047 ± 0.173	2108 ± 479	0.64 ± 0.15
Fe XXV (6637-6700)	1.851–1.868	6.656 ± 0.071	0.273 ± 0.110	211 ± 91	0.06 ± 0.03
Fe II– XVII(7080–7196)	1.72–1.75	7.030 ± 0.080	0.680 ± 0.153	602 ± 189	0.15 ± 0.05

ergy observations from *BeppoSAX* (Matt et al. 1999) and *RXTE*. The modeling is based on the following observations: (a) the 2–10 Å continuum is flat, in F_λ, at long wavelengths (as expected from an "ionized mirror") and hardens below about 5Å (as expected from a "neutral mirror"). This, plus the detection of low ionization species, suggests two distinct components; (b) the EW of the Fe Kα line is very large, indicating iron over abundance (e.g. Netzer et al. 1998); (c) the extended spectrum (outside of the central 0.8″) is flatter than the central spectrum, suggesting that the more neutral component contributes less at larger radii.

Modeling is done using ION00, the 2000 version of the photoionization code ION (Netzer 1996). This includes the computation of the steady state ionization and thermal structure of the gas, and the emergent spectrum. The main ingredients of the model are: (a) Central power-law continuum with $\Gamma = 1.5$, extending from 0.1–100 keV and normalized to produce $L_{2-10\,\mathrm{keV}} = 10^{42}$ erg s^{-1}, in agreement with the *BeppoSAX* and *RXTE* observations; (b) two component gas with twice-solar metallicity. We have experimented with the density and column density of the two and found the following satisfactory combination: 1. An *ionized component* with a radial density distribution of $N(r) = N_0(r/r_0)^{-1.5}$ where $r_0 = 1$ pc and $N_0 = 2 \times 10^3$ cm^{-3}. This distribution is consistent with our measured radial flux distribution assuming most of the 0.8–3″ flux is due to scattered continuum. 2. A *neutral component* with a similar (yet unconstrained) radial distribution with the same r_0, but with $N_0 = 2 \times 10^5$ cm^{-3}. The first component is allowed to extend all the way to 300 pc while the second is limited by its column density, arbitrarily chosen at $10^{23.9}$ cm^{-2}, and is thus terminated well inside the inner 8 pc. This component can perhaps be viewed as the wall of the inner torus. The covering factors of the two components are free parameters of the model; (c) the gas turbulent velocity can range from no turbulence (pure thermal motion) up to $few \times 100$ km s^{-1}. The increased line width results in an increased intensity of all resonance lines due to continuum fluorescence (Krolik and Kriss 1995; Netzer 1996). Our best model requires no turbulent motion.

Several models have been computed, with various covering factors. A satisfactory solution is found for $\Omega/4\pi(neutral) = 0.4$–$0.5$, and $\Omega/4\pi$ (ionized) $= 0.1$–0.2, consistent with the expected opening angle of the (hypothetical) torus, where Ω is the solid angle subtended by the gas to the illuminating source. Figure 1 shows the two components alongside with the observations and Figure 3 shows observed over computed intensities for the strongest lines. Note that, given the gas density and location, the only free parameters are the covering factors of the two components.

The overall agreement between the model and the observations is good, given the uncertainties. In particular: (a) the observed fluxes of most emission lines are reproduced, to within a factor of two. The 1.5–11 Å continuum shape is reproduced too. These results support the idea of the two component model,

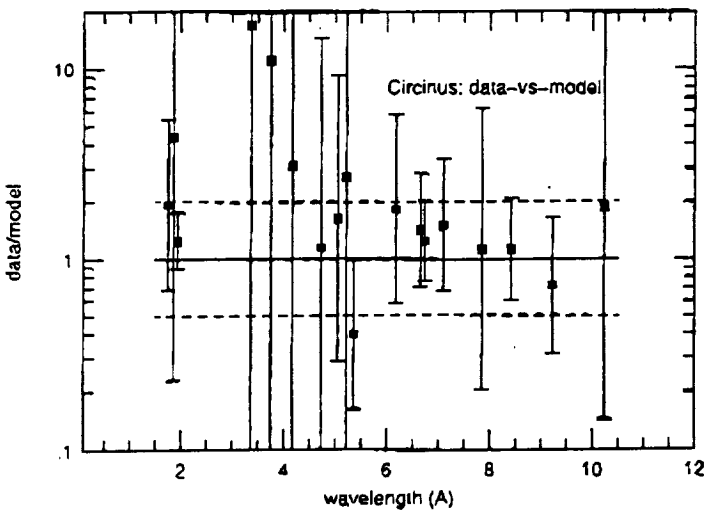

FIG. 3.— A comparison of observed and calculated line intensities. The lines can be identified by their wavelengths. The solid line marks the locus of equality between data and model, the dashed lines represent a factor 2 uncertainty from the solid line.

with the assumed levels of ionization and metallicity; (b) the covering fractions are consistent with the suggested source geometry. The radial density distribution reproduces well the highly peaked emission of this source and the relative weak flux outside the central 16 pc. The calculated scattered continuum and extended emission lines in the inner 16–57 pc are in good agreement with the (highly uncertain, see our companion paper) observations and there is no need to assume an additional starburst source; (c) the "neutral" iron Kα and Kβ lines are consistent with the compact, neutral component gas and the assumed metallicity. Notable difficulties are the over-prediction of the Fe L-shell lines around 9–12 Å and the under-prediction of the 6.6 keV feature if due to Fe XXV. All argon lines are also under-predicted by the model. The measured intensity of these lines are highly uncertain and any suggestion for their origin (e.g. unusual composition) must await better observations. We also note that the predicted Kα flux, outside the central 20 pc, is below the observed value. This may be due to the already noted uncertainty in flux measurement. We also note that a "typical" NLR, can produce a sizeable fraction of this Kα emission.

Regarding earlier X-ray observations of this source, the discovery paper by Matt et al. (1996) reports an *ASCA* spectrum including both neutral and ionized species. Netzer et al. (1998) re-analyzed the *ASCA* data and reported the measurements of six ionized lines plus the iron K-lines, all in reasonable agreement with the present observations. The paper includes a detailed photoionization model of the source and addresses also the Kα/Hβ line ratio. Guainazzi et al. (1999) reported on *BeppoSAX* data that include the measurement of Si XIII, S XV, and Ar XVII lines, as well as neutral Fe-K lines. The observed fluxes are in good agreement except for Ar XVII whose *BeppoSAX* intensity exceeds our estimate by a factor 4.

The present observations, being far superior in terms of the spatial and spectral resolution, yet limited in signal-to-noise ratio, confirm several of the suspected features of this source, such as the gas location, metallicity, and the various components. This, and the recently published *Chandra* observations of Mkn 3 (Sako et al. 2000b) show, for the first time, that centrally illuminated ionized gas in Seyfert 2 galaxies can have very different distributions in different sources. While in Mkn 3 most of the line emission is spread over several hundred parsecs, this in not the case in Circinus, where the ionized gas is highly concentrated near the center and most of its flux originates within the central $\sim$ 15 pc. Moreover, the new observations show that the more neutral gas is even more concentrated, and its dimension may be as small as a few parsecs. While we do not want to speculate about the origin of this difference, we note the large difference in luminosity between these two sources. It is therefore possible that the highly ionized gas in Seyfert galaxies has dimensions that are regulated by the central source's X-ray luminosity.

6. CONCLUSIONS

The new *Chandra* observations of the Seyfert 2 galaxy Circinus enable the very first detailed analysis of the physical conditions and the gas distribution in the inner 200 pc of this source. Our observations show the emission to be highly concentrated within the inner 60 pc and suggest that emission within this volume is entirely due to the reprocessing of the obscured central source's radiation. An even smaller, more neutral component is seen through emission of low ionization iron lines and hard reflected continuum. This is the first determination of the ionized gas distribution in the inner 100 pc region of a Seyfert 2 galaxy.

We acknowledge the financial support of NASA grant NAS8–38252 (RMS; GPG PI), NASA grant NAG5–7276 from *RXTE* AO3, NASA LTSA grant NAG5–8107 (WNB, SK), and the Israel Science Foundation (HN).

REFERENCES

Freeman K.C., Karlsson, B., Lynga, G., Burrell, J.F., van Woerden, H., Goss, W.M., & Mebold, U. 1977, A&A, 55, 445
Guainazzi, M. et al. 1999, MNRAS, 310, 10
Krolik, J. H. & Kriss, G. A. 1995, ApJ, 447, 512
Matt, G. et al. 1999, A&A, 341, L39
Matt, G. et al. 1996, MNRAS, 281, L69
Netzer, H., Turner, T.J., & George, I.M. 1998, ApJ, 504, 680
Netzer, H. 1996, ApJ, 473, 781
Sako, M., Kahn, S.M., Paerels, F., & Liedahl, D.A. 2000a, ApJ, in press (astro-ph/0006146)
Sako, M. et al. 2000b, ApJL, in press (astro-ph/0009323)
Turner, T.J., George, I.M., Nandra, K. & Mushotzky, R.F. 1997, ApJS, 113, 23
Ueno, S., Mushotzky, R.F., Koyama, K., Iwasawa, K., Awaki, H., & Hayashi, I. 1994, PASJ, 46, L71